FULL PAPER

Metabolizable Bi₂Se₃ Nanoplates: Biodistribution, Toxicity, and Uses for Cancer Radiation Therapy and Imaging

Xiao-Dong Zhang, Jie Chen, Yuho Min, Gyeong Bae Park, Xiu Shen, Sha-Sha Song, Yuan-Ming Sun, Hao Wang, Wei Long, Jianping Xie, Kai Gao, Lianfeng Zhang, Saijun Fan, Feiyue Fan, and Unyong Jeong*

Bi, a high atomic number element, has a high photoelectric absorption coefficient, and Se has anticancer activity. Hence, their compound chalcogenide (Bi₂Se₃) deserves a thorough investigation for biomedical applications. This study reveals that Bi₂Se₃ nanoplates (54 nm wide) protected with poly(vinylpyrrollidone) (PVP) could be presumed to have low toxicity even at a high dose of 20 mg/kg in mice. This conclusion is made through studies on the biodistribution and 90-day long term in vivo clearance of the nanoplates. The liver and spleen are dominant organs for accumulation of the nanoplates, which is mainly due to RES absorption. 93% of the nanoplates are cleared after 90 days of treatment. Concentrations of Bi and Se in tumor tissue continuously increased until 72 h after intraperitoneal injection into mice. Such selective accumulation of Bi is utilized to enhance the contrast of X-ray computerized tomography (CT) images. Bi element concentrated in a tumor leads to damage on the tumor cells when exposed to gamma radiation. Growth of the tumor is significantly delayed and stopped in 16 days after the tumor is treated by radiation with Bi₂Se₃ nanoplates. This work clearly shows that Bi₂Se₃ nanoplates may be used for cancer radiation therapy and CT imaging. The nanoplates deserve further study for biological and medical applications.

1. Introduction

Bismuth selenide (Bi₂Se₃) has attracted wide interest in condensed matter physics due to the high thermoelectric figure of merit and the unique surface electronic states as a topological insulator.[1–7] Its biomedical applications, however, have rarely been explored. Se is a natural anticancer element which can inhibit reactive oxygen species.[8] Bi is a high atomic number material (Z = 83) and it has a high photoelectric absorption coefficient (5.3 cm²/g at 100 keV), which is higher than those of I, Au, and Pt. The large X-ray absorption is advantageous for use as a cancer radio sensitizer and X-ray contrast agent.[9–13] Thus, Bi₂Se₃ nanoparticles deserve a thorough biomedical investigation regarding their high radiation enhancement effect and possible use in cancer radiation therapy.

Interactions between nanostructured materials and biological systems are closely related to surface chemistry.[14–23] Nanoparticles without a protected organic layer are agglomerated immediately in blood due to the strong interaction with serum proteins.[13,24] The size of the particle also strongly influences the mechanism of its clearance from the body.[23,25–30] It is well documented that nanoparticles, over the course of prolonged circulation times in the blood, can be continuously accumulated in tumor cells through the enhanced permeability and retention (EPR) of the cancerous cells.[30–35] Coatings of poly(vinylpyrrolidone) (PVP) on nanoparticles has been reported to prolong the circulation, and such nanoparticles have been successfully utilized in X-ray imaging,[36] MRI imaging,[37] and photothermal cancer therapy.[38]

Investigation of the toxicity and clearance of new materials is important for possible medical applications.[39–41] Clearance routes through the liver and kidney are crucial in the metabolism of materials. Nanoparticles smaller than 5.5 nm can be cleared rapidly by renal clearance,[42] while nanoparticles in the range of 10–50 nm can be absorbed by the first-pass extraction from the reticuloendothelial system (RES).[43,44] Nanoparticles larger than 50 nm can be cleared partially by the liver metabolism.[45–48] For example, a recent toxicological investigation in

Dr. X.-D. Zhang, Dr. J. Chen, X. Shen, S.-S. Song, Y.-M. Sun, H. Wang, W. Long, S. Fan, F. Fan
Key Laboratory of Molecular Nuclear Medicine
Institute of Radiation Medicine
Chinese Academy of Medical Sciences and Peking Union Medical College,
Tianjin, 300192, China
Y. Min, G. B. Park, Prof. U. Jeong
Department of Materials Science and Engineering
Yonsei University
134 Shinchon-dong, Seoul, Korea
E-mail: ujeong@yonsei.ac.kr
K. Gao, Prof. L. Zhang
Key Laboratory of Human Disease Comparative Medicine
Ministry of Health, Institute of Laboratory Animal Science
Chinese Academy of Medical Sciences &
Comparative Medical Center, Peking Union Medical College,
Beijing, 100021, China
Prof. J. Xie
Department of Chemical and Biomolecular Engineering
National University of Singapore
10 Kent Ridge Crescent, 119260, Singapore

FULL PAPER
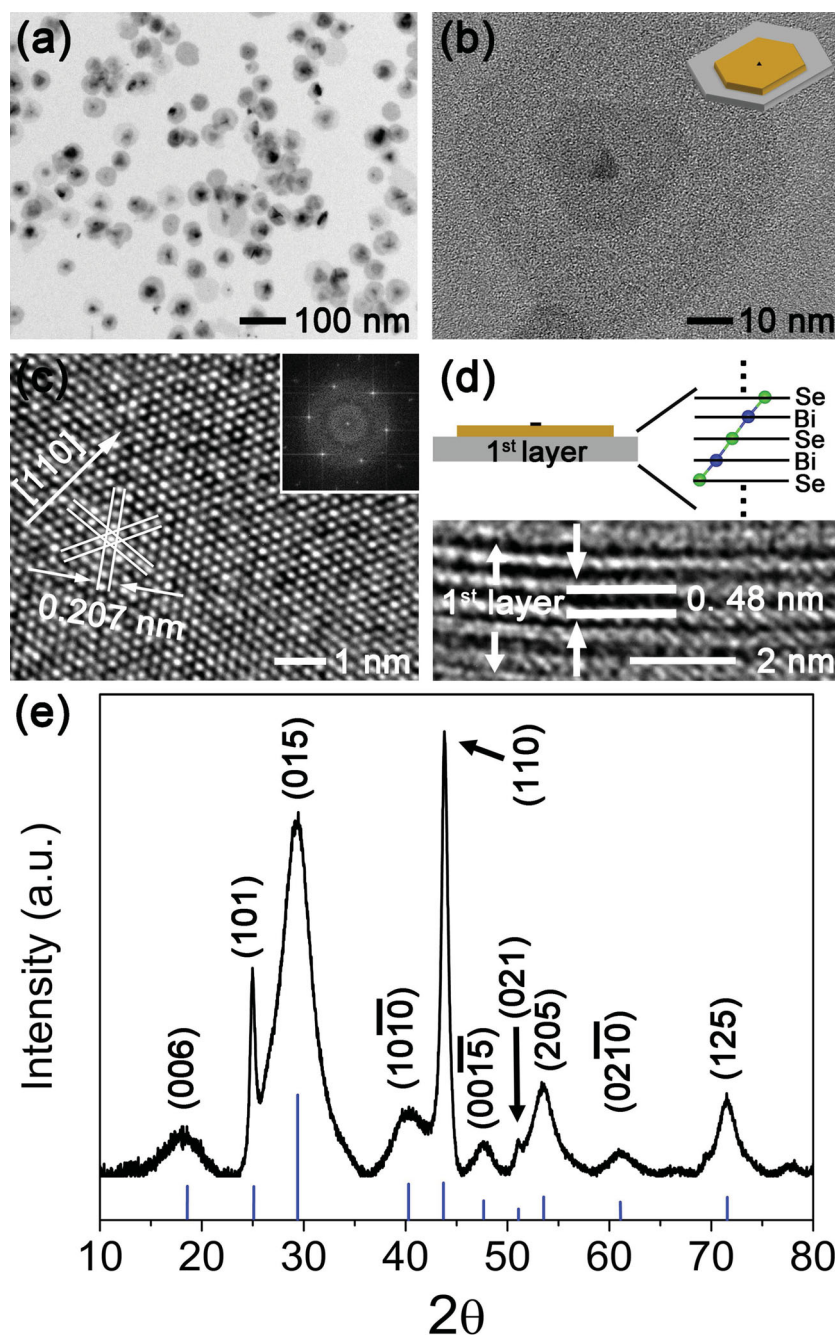
Figure 1. a) Representative TEM image of the PVP-protected Bi_2Se_3 nanoplates (NPs), and b) a magnified image showing a terraced 2D structure of the NPs. c,d) High-resolution TEM image of the as-prepared PVP-protected Bi_2Se_3 NPs in the c) horizontal plane and d) thickness directions. The scheme in Figure 1d shows the bilayered NP with 1QL composed of consecutive five atomic planes. e) XRD image of the as-prepared PVP-protected Bi_2Se_3 NPs. The blue lines are the peaks of bulk Bi_2Se_3.

monkeys showed that 52 nm CdSe quantum dots encapsulated with phospholipid micelles could be partially cleared after 90 days treatment.[49] Thus, searching for metabolizable nanomaterials with efficient biological activity and evaluating their biological response is important for medical application of the materials.

In this work, PVP-coated Bi_2Se_3 nanoplates (NPs, 53.8 nm in width and less than 6 nm in thickness) were employed to investigate their integration into tumor cells and the possibility of their use in cancer radiation therapy and X-ray computed tomography (CT) imaging. The Bi_2Se_3 NPs intraperitoneally injected in mice exhibited continuous accumulation in the tumor cells. The Bi elements in tumors significantly enhanced tumor radiation. Moreover, 90 day long-term toxicological responses showed that 93% Bi_2Se_3 NPs can be metabolized, and no toxicity was found. This work suggests a new method of cancer therapy and CT imaging with Bi_2Se_3 NPs.

2. Results and Discussions

2.1. Analysis of the PVP-Stabilized Bi_2Se_3 Nanoplates

Previously, we have reported the formation of ultra-thin single crystal Bi_2Se_3 nanodiscs and nanosheets in the presence of PVP.[50] We modified the synthesis path to decrease the size of the NPs. Stoichiometric ratio of sodium selenite (Na_2SeO_3) and bismuth nitrate pentahydrate ($Bi(NO_3)_3 \cdot 5H_2O$) were dissolved in ethylene glycol with mild stirring. At 180 °C, reduction was triggered by rapid injection of an ethylene glycol solution of hydrazine hydrate. Details are found in the experimental section. The Bi_2Se_3 NPs were uniformly sized (**Figure 1**a). The thickness of the NPs was the same or less than 4 nm. Average lateral size of the NPs was ~53.8 nm from transmission electron microscopy (TEM) images (Figure S1a) which is consistent with the hydrodynamic diameter (59.8 nm) obtained by dynamic light scattering (Figure S1b). The as-synthesized products were mainly bilayered NPs with a second layer on the primary one, as depicted in the inset of Figure 1b. The structure was already observed in the previous study.[50] Bi_2Se_3 preferentially forms a 2D layered structure. Consecutive five atomic layers stack along the c-axis ($Se_1–Bi–Se_2–Bi–Se_1$) which is a quintuple layer (QL ~ 1 nm).[51] PVP can bind to basal plane composed of negatively charged elemental Se. High-resolution TEM images show the crystal structure of the NPs (Figures 1c,d). The top view TEM image showing the hexagonal lattice fringes with the distance of 0.207 nm (Figure 1c) represents the (110) planes. The cross-section image (Figure 1d) magnifies the side view of 1st primary layer of the bilayered NPs. The lattice spacing of 0.478 nm

© 2013 WILEY-VCH Verlag GmbH & Co. KGaA, Weinheim

FULL PAPER
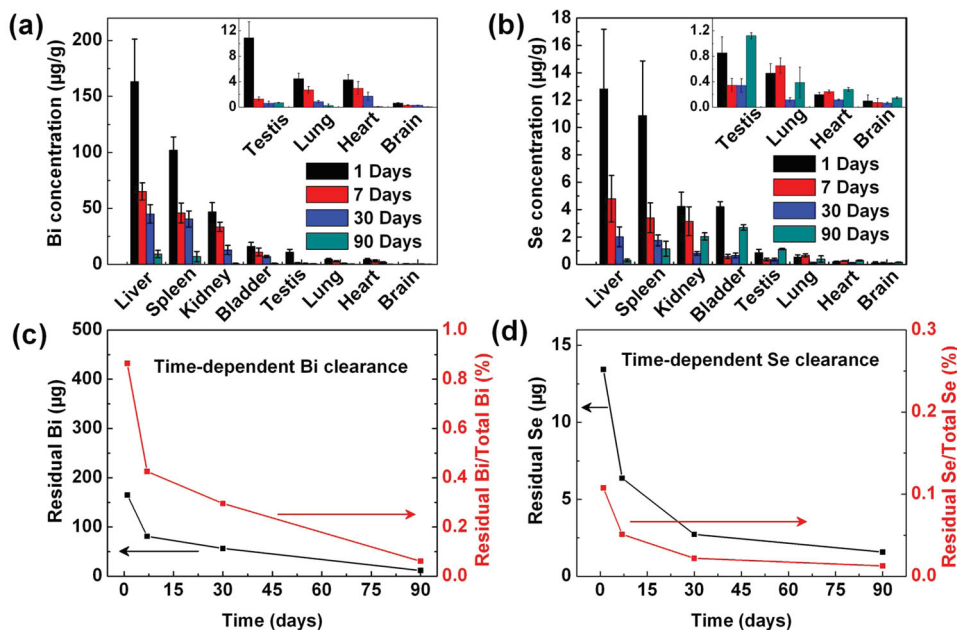
Figure 2. In vivo biodistribution and clearance of the PVP-protected Bi_2Se_3 NPs. a) Bi concentration and b) Se concentration at the different time points of 1, 7, 30, and 90 days after intraperitoneal injection (20 mg/kg). c,d) Residual amount of Bi (c) and Se (d), and the corresponding atomic ratio to the initial atomic amount from the injected Bi_2Se_3 NPs.

corresponds to the (006) plane of Bi_2Se_3. Powder X-ray diffraction (XRD) confirms that the Bi_2Se_3 NPs have the rhombohedral crystal structure with lattice constants of $a = 0.4139$ nm and $c = 2.8636$ nm (Figure 1e). The NPs in this study show a good agreement with the peaks of bulk Bi_2Se_3 with the same crystal structure indicated by the blue vertical lines.[52] The NPs were stabilized by PVP surfactant so that they were dispersed well in water. The zeta potential of the NPs in pure water was −16.69 mV, which is in a regime of stable dispersion. We tested the time-dependent stability of the NPs, and found that hydrodynamic diameter was stable and no significant aggregation was occurred in the phosphate-buffered saline (PBS) after 1 month (Figure S1b). Inspired by these results, we tested the biological response of the Bi_2Se_3 NPs in mice.

2.2. Biodistribution and Clearance of the Bi_2Se_3 Nanoplates

Knowledge of the biodistribution and clearance of a material is critical for its use in medical treatment and possible long-term toxicity. The NP solution (2 mg/mL, 0.2 mL) was injected intraperitoneally into C57 male mice (64 mice, 8 per group). The final dose in the mice was 20 mg/kg. The mice were scarified after 1, 7, 30, and 90 days, and the main organs from three mice per group were tested by inductively coupled plasma mass spectrometry (ICP-MS) and the biodistributions of Bi from the PVP-protected Bi_2Se_3 NPs were obtained (**Figure 2**a). It is clear that the liver, spleen, and kidney are the main target organs, and the bladder and testes are the next. The heart, lung, and brain showed relatively low Bi concentrations. Bi concentration was as high as 163.2 μg/g in the liver, 101.9 μg/g in the spleen, and 46.8 μg/g in the kidney after 1 day. After 90 days, Bi

concentration decreased to 9.26 μg/g in the liver, 6.93 μg/g in the spleen, and 0.78 μg/g in the kidney. Biodistributions of Se in all organs are presented in Figure 2b. After 1 day treatment, Se also showed the highest uptake in liver, spleen, and kidney, with concentrations of 12.8, 10.9, and 4.25 μg/g, respectively. After 90 days, Se concentration decreased to 1.83 μg/g in the liver, 0.23 μg/g in the spleen, and 0.42 μg/g in the kidney. The PVP layer induced a long blood circulation time of the NPs.[53,54] It is not surprising that NPs larger than 10 nm can enter the excretion system through the RES process. Phagocytosis by the Kupffer cells and spleen macrophages is significantly dependent on particle size: the larger particles can induce greater uptake by RES.[44,55] Further, it can be noticed that the Bi concentration in all organs decreased with the increase in treatment days, which indicates time-dependent clearance effects (Figure 2a). Se was detected mainly in the liver, spleen, kidney, and bladder. Se concentration decreased in the organs until 30 days, but increased in kidney, testes, and bladder after 90 days.

To investigate the clearance in detail, the time-dependent residual amount in mice from the injected Bi_2Se_3 NPs was investigated (Figure 2c,d). Residual amounts of Bi and Se in mice were calculated by summing the Bi and Se amount in all organs from Figure 2a and b, respectively. The ICP-MS measurements showed that the initial total amounts of Bi and Se were 190.76 and 124.68 μg, respectively. The residual ratios of Bi and Se were calculated by the residual amount/initial total amount. It was found that the residual amount of Bi in the body after 1 day was 164.95 μg, and it was decreased to 11.66 μg after 90 days, which corresponds to 86.5% of the initial amount after 1 day and 6.1% after 90 days. Similar behavior was observed for Se. The residual amount was 13.43 μg after 1 day, and it decreased to 1.58 μg after 90 days, which indicated 10.8%

www.MaterialsViews.com

ADVANCED
FUNCTIONAL
MATERIALS
www.afm-journal.de

FULL PAPER
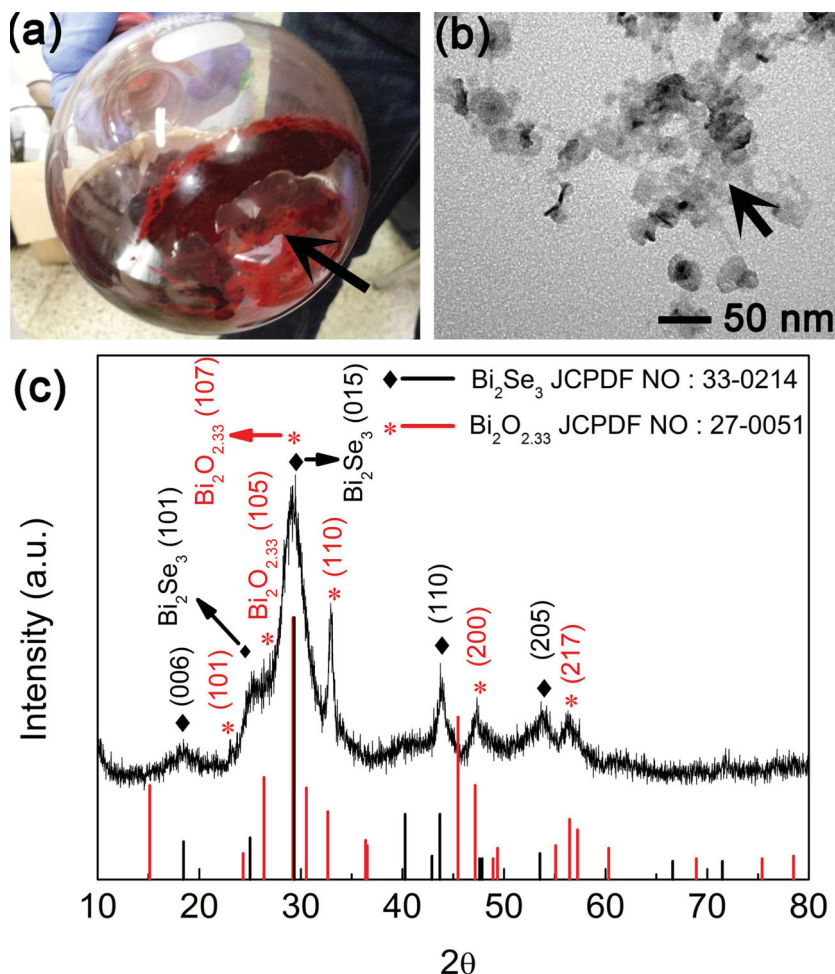
Figure 3. Oxidation of the Bi$_2$Se$_3$ NPs in a PBS buffer solution exposed to air for 30 days. a) Digital image of the NP suspension. The red-colored material precipitated on the bottom surface of the flask is amorphous Se (indicated with an arrow); b) TEM image showing deformation of the NPs by oxidation (indicated by an arrow), and; c) XRD spectrum of the NPs collected from the PBS buffer solution by vacuum filtration. The black vertical lines and the red vertical lines at the bottom represent XRD peaks of pure Bi$_2$Se$_3$ and Bi$_2$O$_{2.33}$.

energy dispersive spectrometer (EDS). The Bi$_2$Se$_3$ NPs were found to be oxidized easily in air. We found that the dry Bi$_2$Se$_3$ NPs powder was oxidized slowly to form Bi$_2$O$_{3-x}$, and the pure Se was phase-separated to form large aggregates. The same oxidation process was observed in the phosphate buffered saline (PBS) solution (pH = 7.4). The Bi$_2$Se$_3$ powder suspended in the PBS buffer solution showed a slow oxidation process when exposed to air. We could not detect traces of oxidation within a few days, however, severe oxidation was observed after one month. As seen in **Figure 3**a, the red amorphous Se was dissolved in the buffer solution and then precipitated on the glassware (indicated with an arrow). A TEM image (Figure 3b) presents the shape deformation of the NPs into irregular amorphous-like particles, which is due to the existence of amorphous Se (indicated with an arrow). The XRD peaks (Figure 3c) correspond to a mixture of Bi$_2$O$_{2.33}$ and residual Bi$_2$Se$_3$, which confirms the replacement of Se by oxygen. Therefore, the as-synthesized NPs were preserved in an Ar environment to prevent possible oxidation. The NPs, before injection, were identical in chemical composition and crystal structure to the as-synthesized ones.

The surprising mismatch of the atomic ratio before and after injection indicates fast oxidation of the NPs in the mouse body. We performed two ICP-MS measurements of the Bi$_2$Se$_3$ nanoplates. The nanoplates were introduced to the blood plasma in vitro and the plasma samples for ICP-MS measurement were taken at time points of 24 and 72 h after ultracentrifugation. It was found that the Bi concentration in the plasma did not noticeably increase, but the Se concentration sharply increased. The weight ratio of Bi/Se rapidly increased to 9.8 after 0.5 h, and further increased to 11.7 after 24 h (**Figure 4**a). These results confirm the fast oxidation of the NPs, which dissolve Se in the mouse blood. We further confirmed it by in vivo experiment: after in vivo injection, the Bi concentration sharply increased after 1 h and then decreased rapidly. In contrast, the Se concentration reached a relatively stable level. The Bi/Se atomic ratio reached 5:1 after 1 h, but it decreased rapidly to 0.2 after 72 h (Figure 4b). Figure 4c schematically depicts the oxidation process in blood. The oxidized NPs or pristine NPs were absorbed by RES, but Se atoms dissolved in the blood remained in the blood plasma, probably existing in complex forms with the biomolecules in the blood, allowing Se to circulate for a long time in blood. Further, the Se dissolved in blood could be metabolized by renal clearance and thus accumulates in the bladder.[42,58,59] A similar phenomenon has been reported in previous work where PEG-coated gold NPs presented accumulation in organs after 90 days treatment.[45]
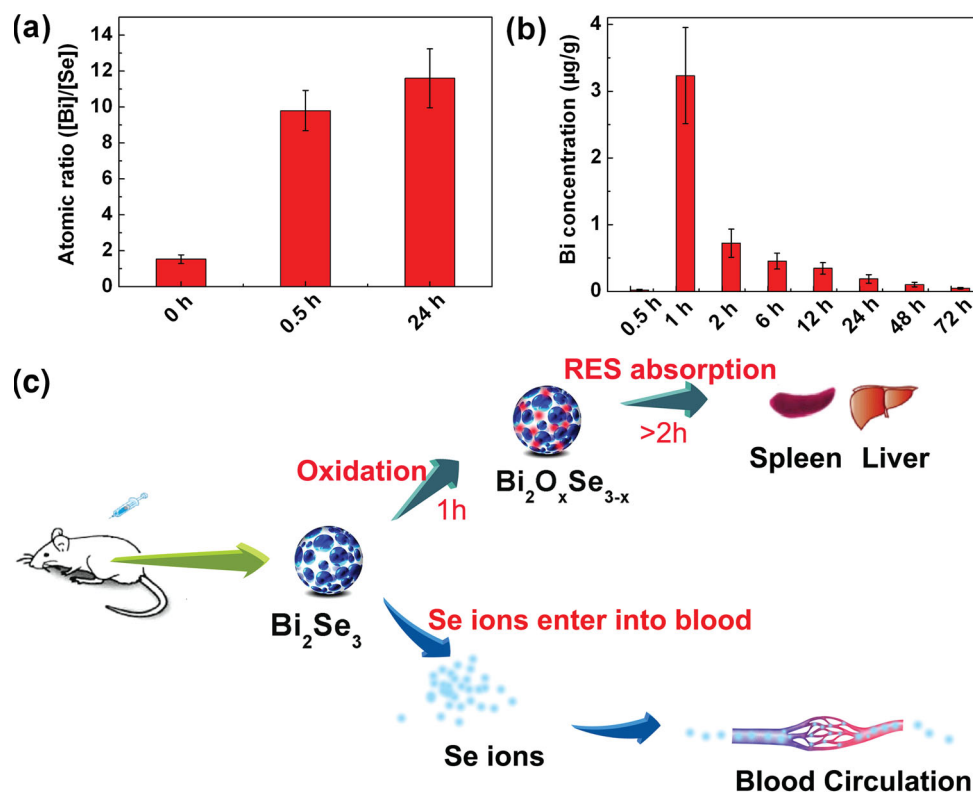
after 1 day and 1.3% after 90 days. It is proposed that small NPs below 5.5 nm can be cleared by the kidney, while large NPs above 50 nm may be partially cleared by the liver as the time increases.[42] Thus, clearance by the liver is a significant contribution to the decrease of Bi$_2$Se$_3$ NPs in mice. Meanwhile, it is worth noting that high concentrations of Bi and Se can also be found in the kidney, indicating that the kidney may participate in the partial metabolism of the NPs. It is similar to the previous work, in which 50 nm Au particles showed an unexpected high distribution in kidney.[44] Indeed, it was demonstrated that 10–30 nm graphene nanosheets could be cleared by both liver and kidney.[56,57] However, it is not clear whether metabolism of other organs is related to the breakdown of NPs in vivo. The NPs indeed can be degraded and excreted with long time blood circulation and physiological environment.[47]

It is notable that from the results in Figure 2, the Bi concentration was about 10 times higher than that of Se concentration. The as-synthesized Bi$_2$Se$_3$ NPs were stoichiometric, with a Bi/Se ratio of ~1.53 that was obtained from ICP-MS and

Figure 4. Oxidation process of Bi_2Se_3 NPs. a) Time-dependent atomic ratio of Bi to Se in vitro. b) Time-dependent concentration of Bi which was measured by ICP-MS in vivo. c) Illustration to describe the dissolution and oxidation of the Bi_2Se_3 NPs after intraperitonal injection.

2.3. Toxicity of the Bi_2Se_3 Nanoplates

We next investigated the in vivo toxicity of Bi_2Se_3 NPs at the dose of 20 mg/kg by evaluating body weight, immune response, hematology, and biochemistry at the time points of 1, 7, 30, and 90 days. During the 90 day period, the treatment with Bi_2Se_3 NPs did not cause obvious adverse effects on growth, and no meaningful statistical differences were observed in body weight and thymus index between the Bi_2Se_3 NP-treated mice and control mice (Figure S2a,S2b). Spleen index in the NP-treated mice increased steadily up to 30 days, but had decreased after 90 days (Figure S2c). We selected standard hematology markers for analysis, including white blood cell (WBC), red blood cell (RBC), hematocrit (HCT), mean corpuscular volume (MCV), hemoglobin (HGB), platelet (PLT), mean corpuscular hemoglobin (MCH), and mean corpuscular hemoglobin concentration (MCHC). Hematology results for the Bi_2Se_3 NPs are presented in **Figure 5**a. For the NP-treated mice, two typical indicators (WBC, RBC) did not show meaningful differences from those of the untreated mice. PLT increased after 30 days treatment, but recovered after 90 days treatment. Other parameters (MCV, MCH, MCHC, HGB, HCT) had no significant difference. These results indicate limited biological damage to the mice. When the NPs were injected into the mice, they would interact with all serum proteins, such as albumin, fibrinogen, γ-globulin, histone, and insulin. The blood chemistry of mice has not been affected directly. The PVP-protected layer plays

the role of a blood compatible surface coating layer, which is consistent with the previous works.[36,60] Compared with the Au-based nanomaterials at a similar dose range (10~20 mg/kg), the PVP-protected Bi_2Se_3 NPs caused a less toxic responses. The PEG-coated Au NPs resulted in acute increases of RBC and WBC by intraperitoneal and oral injections because RBC and WBC are sensitive to infection and inflammation caused by the Au NPs.[43,45,59,61–63] These results show that the PVP-protected Bi_2Se_3 NPs do not cause significant infection and inflammation for mice.

Furthermore, we performed the standard biochemistry examination with the mice treated by the Bi_2Se_3 NPs at the different time points of 1, 7, 30, and 90 days (Figure 5b). The biochemical parameters including i) alanine transaminase (ALT), ii) aspartate transaminase (AST), iii) total protein (TP), iv) albumin (ALB), v) blood urea nitrogen (BUN), vi) creatinine (CREA), vii) globulin (GLOB), and viii) total bilirubin (TBIL) were investigated. We emphasize ALT, AST, and CREA because they are closely related to the functions of the liver and kidney of mice. Meaningful changes were not observed in all parameters after 1 day. The NPs presented appreciable liver accumulation after 1 day, but did not cause acute injury at this time point. After 7 days treatment, ALT significantly increased in the NP-treated mice, while AST and CREA did not have noticeable difference in the treated mice. After 90 days, ALT has changed back to a normal level which indicates that the Bi_2Se_3 NPs caused slight damage for liver after 7 days, but the damage recovered after
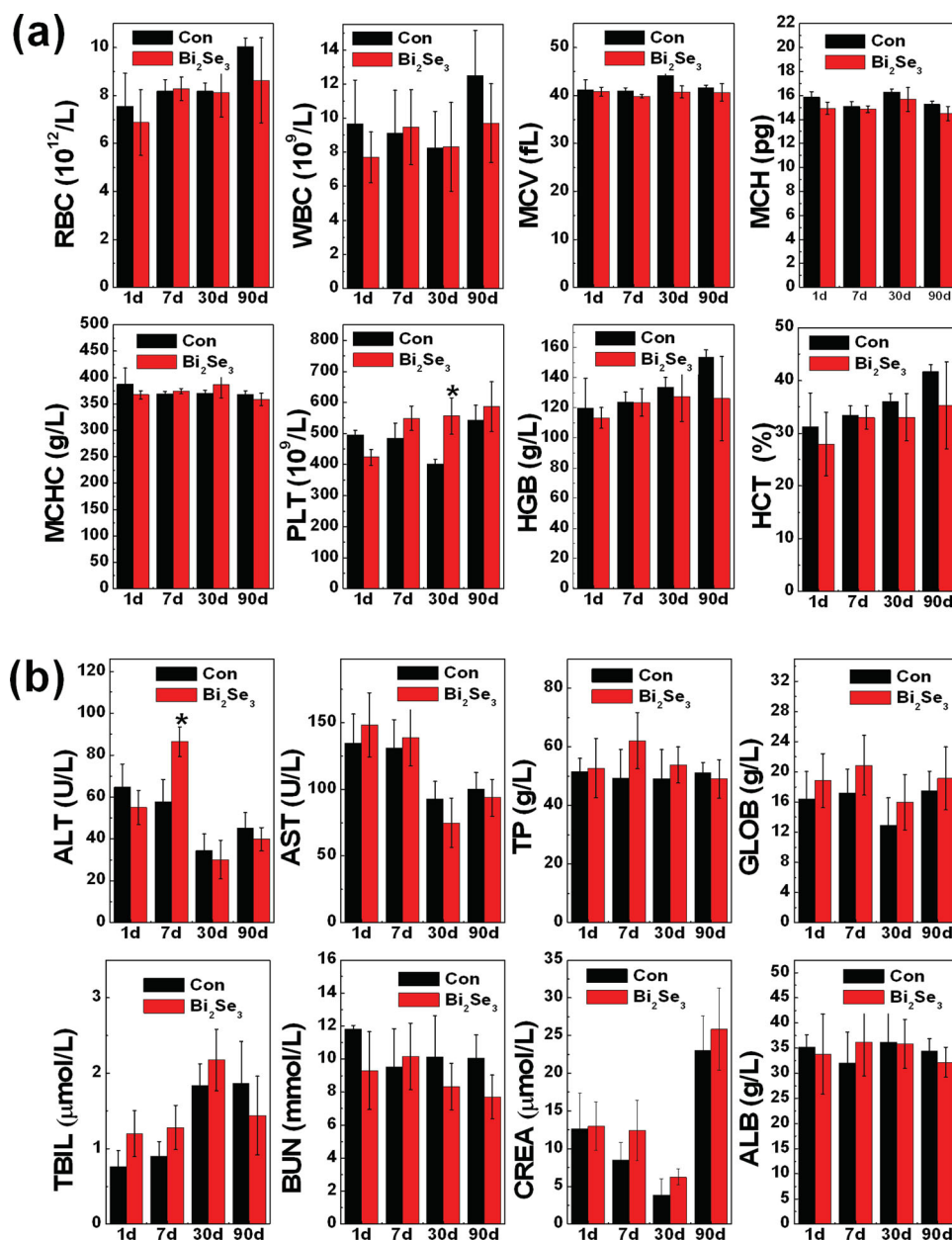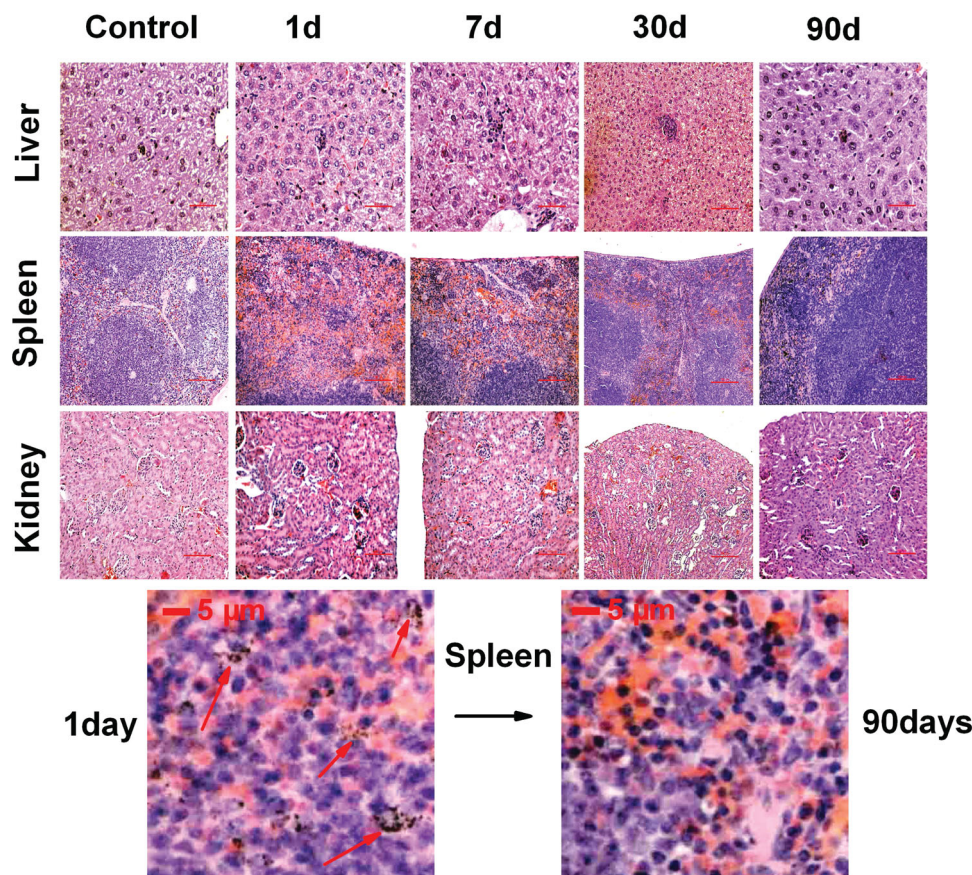
Figure 5. a) Hematology data of the mice treated with the PVP-protected Bi_2Se_3 NPs. The data were collected at the different time points of 1, 7, 30, and 90 days after intraperitoneal injection (20 mg/kg). The terms are following: red blood cells (RBC), white blood cells (WBC), platelets (PLT), mean corpuscular hemoglobin (MCH), mean corpuscular hemoglobin concentration (MCHC), mean corpuscular volume (MCV), hemoglobin (HGB), and hematocrit (HCT). The terms 'Con.' and 'Bi_2Se_3' in the figures indicate controlled mice without the Bi_2Se_3 NPs and the mice treated with the NPs, respectively. b) Blood biochemistry analysis of the mice treated with the PVP-protected Bi_2Se_3 NPs at the different time points of 1, 7, 30, and 90 days. The results show mean and standard deviation of aminotransferase (ALT), aminotransferase (AST), total protein (TP), albumin (ALB), blood urea nitrogen (BUN), creatinine (CREA), globulin (GOLB), and total bilirubin (TBIL). Data were obtained by Student's t-test.

30 and 90 days, respectively. It is consistent with the biodistribution and clearance of the NPs. It is widely reported that the liver accumulation of Au and metal oxide nanomaterials can induce a continuous increase of ALT and AST, and thus significant damage in the liver. Even at the dose level of 5 mg/kg through intravenous injection, Au nanoparticles and nanoclusters stabilized by PEG and BSA caused acute damage even after 90 days.[59,61] Similarly, PEG- and oleic acid-coated Fe_3O_4

nanocrystals with sizes of 5–30 nm led to steady increases of ALT, AST, and BUN at doses of 5–7.5 mg/kg.[64] However, the Bi_2Se_3 NPs showed very low liver toxicity even at a 20 mg/kg dose.

Finally, we checked the pathological changes of organs by using immunohistochemistry at different time points. We collected liver, spleen, and kidney, and sliced them for Haematoxylin and Eosin (H&E) staining (**Figure 6**). No significant organ

Figure 6. Pathological data from the liver, spleen, and kidney of the mice treated with the PVP-protected Bi$_2$Se$_3$ NPs. The data were collected at different time points of 1, 7, 30, and 90 days after injecting a 20 mg/kg dose.

damage was observed in the spleen or kidney during the whole treatment period. Slight pathological change was shown in the liver after 7 days treatment, but it recovered to the normal state after 90 days treatment. No noticeable toxic effects were detected in the heart, lung, testis, bladder, or brain (Figure S3). Another feature of pathology is to qualitatively investigate the clearance of the Bi$_2$Se$_3$ NPs.[57,64] When the NPs are accumulated in an organ, they may aggregate and permit direct observations through an optical microscope. A large number of dark spots (less than 1 μm) were found in the spleen after 1 and 7 days treatment, but they were cleared after 90 days. Similar results were reported for carbon nanotube-, graphene-, and Fe$_3$O$_4$ NP-treated mice. Black spots were observed in the liver, but they eventually disappeared after about 90 days.

Currently, nanomedicine is searching for materials with low toxicity and highly efficient clearance. It is widely accepted that small-size nanoparticles can be cleared by the kidney. The actual situation, however, is far more complex than the expectation. A case in point is the clearance of Au nanoparticles. The PEG-protected Au nanoparticles (3 nm) could not be cleared, but glutathione (GSH)-protected Au nanoparticles with the same size showed efficient renal clearance.[59,65] Carbon materials could be gradually cleared by the kidney and liver when the size was up to 10~30 nm.[57] Therefore, it is shown that the clearance of nanomaterials is not only related to size and

surface chemistry, but also related to the shape and stability. Exploring the clearance of large-size materials provides another viable route for the design of metabolizable nanomaterials. The present work clearly shows that the PVP-protected Bi$_2$Se$_3$ NPs can be metabolized by the liver, hence they show large promise for medical applications such as use as contrast agents and in cancer therapy.

2.4. Cancer Radiation Therapy with Bi$_2$Se$_3$ Nanoplates

The cell responses (or biocompatibility) of the PVP-protected Bi$_2$Se$_3$ NPs were evaluated using HeLa cells. The HeLa cells were treated with Bi$_2$Se$_3$ NPs with different concentrations of 1.56~200 μg/mL. As shown in **Figure 7**a, the viabilities of the cells changed very little after 24 h and 48 h as the concentration of the NPs was increased, which indicates a low cytotoxicity even at a high dosage of 200 μg/mL. The in vitro radiation enhancement of the Bi$_2$Se$_3$ NPs was measured by MTT assay using the HeLa cells. As shown in Figure 7b, obvious enhancement in radiation with increasing dosage was observed for the cell cultures treated with the Bi$_2$Se$_3$ NPs. The radiation enhancement is regarded to be caused by increased DNA damage induced by the photoelectric effect and Compton scattering of the heavy metal (Bi).[66,67] This hypothesis was confirmed by a single-

www.MaterialsViews.com

ADVANCED
FUNCTIONAL
MATERIALS
www.afm-journal.de

FULL PAPER
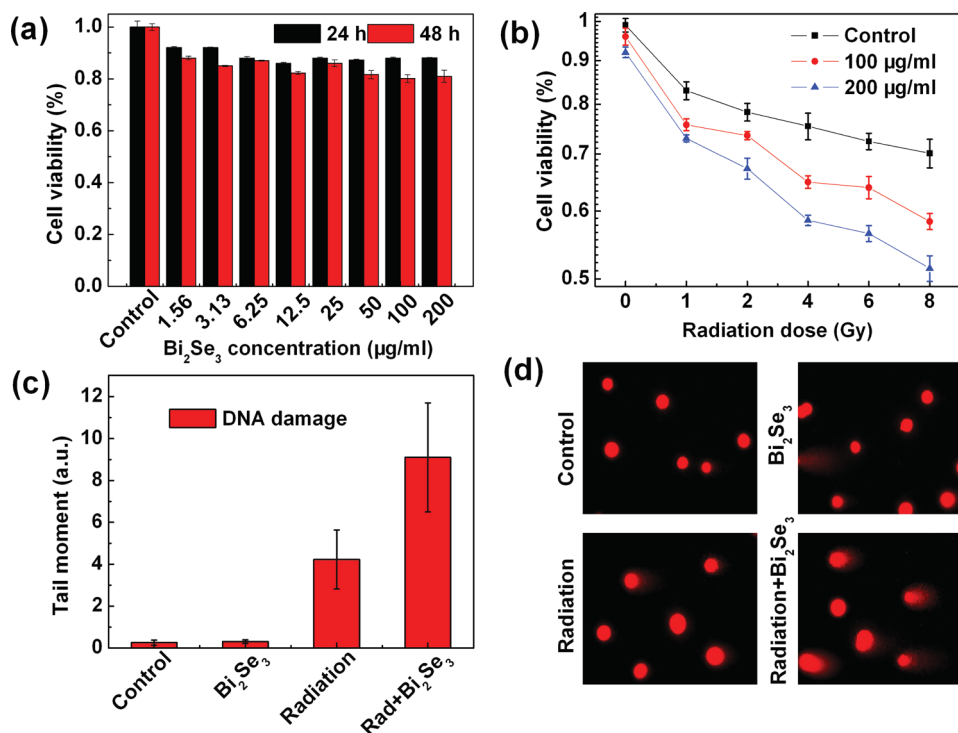
Figure 7. a) Viability of HeLa cells after incubation with the PVP-protected Bi_2Se_3 NPs for 24 and 48 h. b) Viability of HeLa cells treated with only radiation [control, black line], the Bi_2Se_3 NPs (100 μg/mL) + radiation [red line], and the Bi_2Se_3 NPs (200 μg/mL) + radiation [blue line]. c) Tail moment of HeLa cells treated with the Bi_2Se_3 NPs, radiation (3 Gy), and the Bi_2Se_3 NPs + radiation (3 Gy). d) Representative cell images of fluorescent DNA stain of control, radiation group, the Bi_2Se_3 NPs, and the Bi_2Se_3 NPs + radiation (3 Gy).
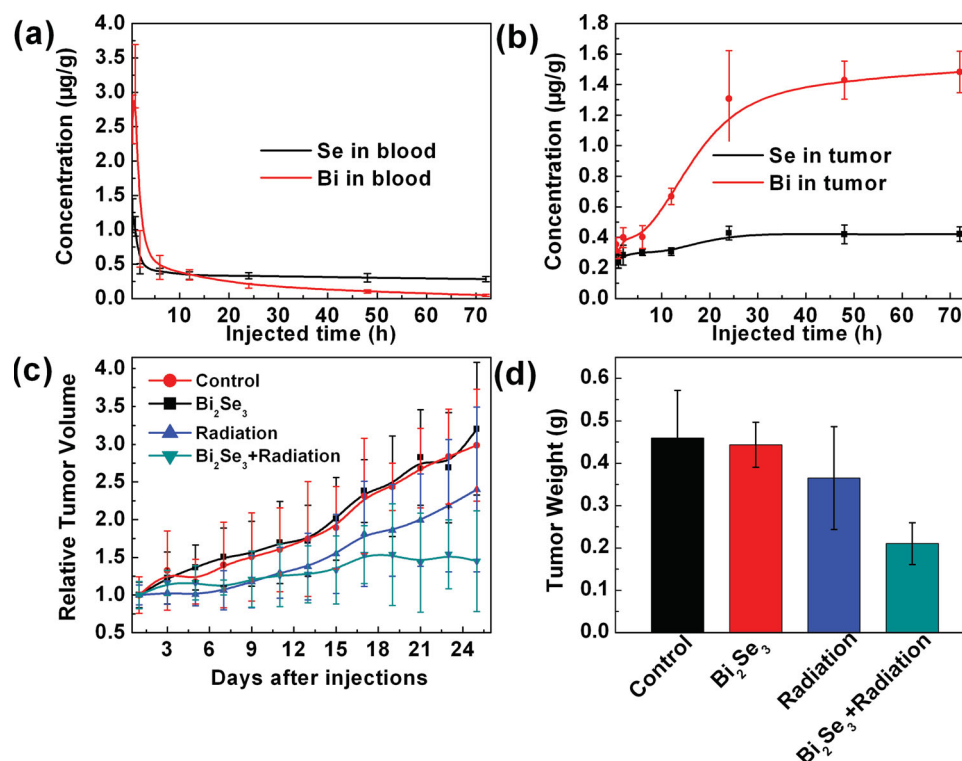
cell gel electrophoresis study. Without radiation, negligible DNA damage was observed for the cell treated with the NPs (Figure 7c). In contrast, after receiving a 3 Gray (Gy) radiation dose, the DNA damage in the NP-treated culture was much more significant than in the untreated culture (Figure 7c). The remarkable DNA damage was also confirmed by in vitro imaging via the fluorescent DNA stain (Figure 7d). Long tails observed in the stain indicate significant DNA damage. There was no obvious DNA damage without radiation in both cells with/without NP treatment, while long tails of stain were easily observed in the cells of the NP-treated culture after 3 Gy radiation. Bi_2Se_3 NPs could be assumed to have low toxicity and can clearly enhance DNA radiation damage. Radiation enhancement of the Bi_2Se_3 NPs is comparable with Au nanoparticles.[59]

Inspired by these results, we next investigated the in vivo biodistribution of the PVP-protected Bi_2Se_3 NPs using U14 tumor-bearing male nude mice (24 mice, 3 per group) after intraperitoneal injection (2 mg/mL, 0.2 mL) at the dose of 20 mg/kg. We used ICP-MS to measure the concentrations of Bi and Se in blood at different time points of 0.5, 1, 2, 6, 12, 24, 48, and 72 h (**Figure 8**a). The concentrations of both Bi and Se sharply decreased in the first phase, and then gradually decreased in the second phase. In the first phase, the blood concentrations decayed to half in 1.9 h for Bi and in 1.5 h for Se. The blood circulation times were lower that of 10–40 nm PEG-coated Au particles,[43,68,69] but higher than those of quantum dots.[32,68,70,71] Time-dependent concentrations of Bi and Se in tumor tissues were obtained from the same mice (Figure 8b). The Bi

concentration in the tumor gradually increased from 0.35 μg/g (1.75% ID/g) in 0.5 h to 1.48 μg/g (7.4% ID/g) in 72 h, and then approached a plateau value in ~24 h. The concentration of Se in the tumor tissue increased from 0.25 μg/g in 0.5 h to 0.42 μg/g in 72 h. It is definite that the uptake into the tumor of the NPs accumulated in tumor tissue by the passive targeting effect, which is consistent with previous works.[72,73] Further, it is found that the Bi concentration was close to the reported values of the Au nanoparticles (6.25% ID/g) and the Au nanorods (7% ID/g) accumulated in tumor tissues in 72 h after injection with the same dose.[68,69,71]

Encouraged by the highly effective accumulation of Bi in tumor cells, in vivo cancer radiation therapy was carried out by using U14 tumor-bearing nude mice. The PVP-protected Bi_2Se_3 NPs were intraperitoneally injected into mice (20 mg/kg). After 24 h, the mice were locally irradiated under ^{137}Cs gamma radiation of 3600 Ci at the dose of 5 Gy. The volume of the tumor was monitored by the Student's T-test (Figure 8c). Without the radiation treatment, the tumor volume at the beginning steadily increased by 3.2 times after 25 days, regardless of the existence of the NPs. With the radiation treatment, the growth of the tumor volume in the mice without NP injection (radiation only) was retarded by 6 days, but the tumor eventually grew to 2.4 times after 25 days. The tumor volume of the NP-treated mice with radiation was 1.47 times after 25 days, which is a significant reduction in growth rate. It is notable that the tumor volume did not increase after 16 days until 25 days. Similarly, the tumor weight of the mice treated with NPs plus radiation

FULL PAPER

ADVANCED
FUNCTIONAL
MATERIALS
www.afm-journal.de

Materials Views
www.MaterialsViews.com

Figure 8. In vivo biodistribution and passive targeting of the PVP-protected Bi_2Se_3 NPs. Concentration of Bi and Se in blood (a) and in tumor (b) at the different time points of 0.5, 1, 2, 6, 12, 24, 72 h after intraperitoneal injection (20 mg/kg). Time-course studies of the tumor volume (c) and the tumor weight (d) of mice treated with the PVP-protected Bi_2Se_3 NPs at the concentration of 20 mg/kg. Data was obtained by the Student's t-test.

exhibited a net increase of 0.1 g from the initial weight (0.21 g), which was less than the control mice and the mice with radiation only (Figure 8d). These in vivo results present that the PVP-protected Bi_2Se_3 NPs have a strong radiation enhancement effect and may be used as a radiosensitizer. Cancer radiation therapy of heavy metal elements mainly depends on the concentration in tumor and the photoelectric absorption. The photoelectric absorption coefficient of Bi is 0.12 cm^2/g at radiation energy of 600 keV which is higher than that of Au (0.08 cm^2/g) at the same radiation energy. The effective accumulation in tumor tissue and the unique X-ray absorption induce obvious inhabitation of tumor growth after radiation.[74]

2.5. X-Ray CT Imaging with Bi_2Se_3 Nanoplates

We next performed in vivo X-ray CT imaging of the Bi_2Se_3 NPs in the mice bearing U14 tumors. The Bi_2Se_3 NPs (100 mg/mL, 0.2 ml) were intraperitoneally injected before anaesthesia. Both 3D and 2D CT imaging were used to evaluate the tumor uptake and clearance (**Figure 9**). 3D imaging reveals the tumor outlines and boundaries of the tumor sites (indicated by the red circle) 24 h after the injection of the Bi_2Se_3 NPs (Figure 9a). The Bi_2Se_3 NPs were also observed in the bladder (Figure 9 b), which indicates that the NPs were partially cleared by kidney. Figure 9c–e show time-dependent 2D CT imaging of the Bi_2Se_3 NPs. The tumor boundary was not clear at 3 h, but it was discriminated gradually as the time increased to

24 h, which is attributed to the passive accumulation of NPs in the tumor. Figure 9f–h show the bladder. The bladder was seen clearly at 3 h and started to lose its intensity after 24 h, which indicates the time-dependent renal clearance effect. It was reported that small particles (<5.5 nm) can be cleared by the kidney.[42,58,59] Our work, however, suggests that the Bi_2Se_3 NPs can also be metabolized partially by renal clearance. The X-ray CT imaging is related to the atomic number and relative ratio of organ/muscle. Au nanoparticles were reported to be used as X-ray contrast agents at a concentration of 100 mg/g.[75,76] In our work, X-ray CT imaging with the Bi_2Se_3 NPs could exhibit the clear boundary between tumor and normal tissue at similar concentrations to the Au nanoparticles.

3. Conclusion

This study explored the distribution of the Bi_2Se_3 nanoplates (NPs) (53.8 in width, 6 nm in thickness) in the U14 tumor-bearing male mice. The NPs stabilized with PVP exhibited a long blood circulation half-life (>50 h). We investigated the in vivo toxicity, biodistribution, and clearance of the PVP-protected Bi_2Se_3 NPs at a dose of 20 mg/kg. It was found that the liver and spleen were main target organs. A large amount of Bi was found in the liver and spleen after 1 day treatment (~163.2 µg/g in liver, ~101.9 µg/g in spleen), but more than 93% of the Bi was cleared after 90 days treatment. The concentrations of Bi and Se in the organs significantly decreased after 25 days, but
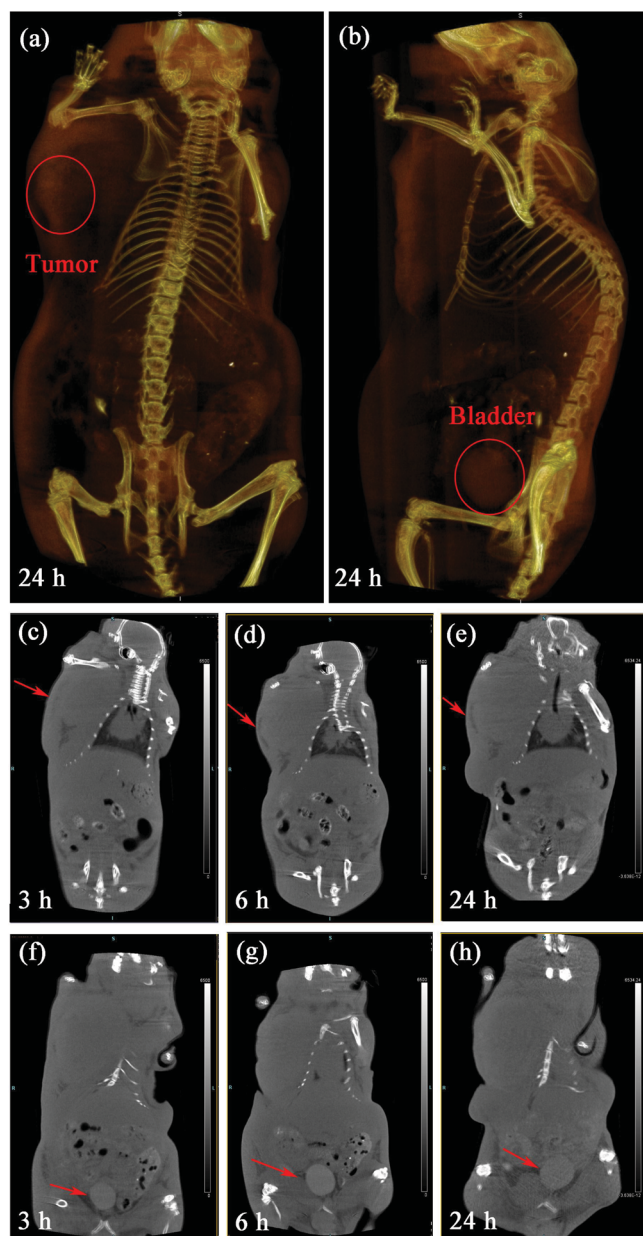
Figure 9. 3D in vivo X-ray CT imaging of tumor tissue (red circle) and bladder (red circle) from the PVP-protected Bi$_2$Se$_3$ NPs from front view (a) and from side view (b) at 24 h. c–e) 2D images of the tumor tissue (red arrow) were taken at c) 3 h, d) 6 h, and e) 24 h. f–h) 2D images of the bladder (red arrow) from PVP-protected Bi$_2$Se$_3$ NP-treated mice at f) 3 h, g) 6 h, and h) 24 h.

the accumulation of Bi in the tumor cells increased through the enhanced permeability and retention (EPR) of the cancerous tumors. The Bi elements accumulated in the tumor cells were employed as a radiosensitizer to inhibit the growth of the cancer cells and enhance the contrast in computerized tomography. Once treated with the NPs and radiation, the growth of the cancer cells was significantly delayed and the cancer cells did not grow further after 16 days. This work suggests a new method of radiation cancer therapy employing the Bi$_2$Se$_3$

nanoplates. The effect of diverse surface stabilizers on the circulation time and biodistribution of Bi in the tumor cells is left for future study.

4. Experimental Section

Materials and Synthesis: 1.0 g of poly(vinylpyrrolidone) (PVP, M$_w$=55 000, Sigma-Aldrich) was dissolved in 50 mL of ethylene glycol (EG, ≥99%, J. T. Baker), and the solution was poured in 250 mL round-bottom flask. A solution of sodium selenite (99%, Aldrich, 0.242 g in 40 mL of EG) and a solution of bismuth nitrate pentahydrate (99.99+%, Aldrich, 0.452 g in 15 mL of EG) were added to the PVP solution under magnetic stirring at room temperature. The flask was sealed and heated to 180 °C in nitrogen environment. As the reaction temperature increased, transparent reaction mixture became milky white and turned yellow-white. Hydrazine hydrate solution (2 mL in 20 mL of EG) was rapidly injected to the mixture by a syringe. The reaction mixture turned dark immediately, which indicates the formation of the PVP-protected Bi$_2$Se$_3$ NPs. The reaction was allowed to proceed for 30 min for a complete reaction and cooled down to room temperature. The final products were precipitated by centrifuging (12 000 rpm, 10 min) and washed three times with a mixture of acetone (300 mL) and deionized (DI) water (60 mL). And, the precipitate was washed with pure DI water twice and dried in vacuum.

Material Characterization: Transmission electron microscope (TEM) analysis was conducted at 200 kV with JEOL models (JEM-2100F and JEM-2011HC). X-ray diffraction (XRD) measurement was performed with a Rigaku D/MAX II X-ray diffractrometer at Cu K$_\alpha$ radiation (λ = 0.1542 nm). The scanning range extended from 10 to 80° with a speed of about 3°/min. The zeta-potential was measured by electrophoretic measurements (ELS-Z2). Size distribution of the Bi$_2$Se$_3$ NPs was determined with the NanoZS Zetasizer particle analyzer (Malvern). Sample solutions were prepared by diluting Bi$_2$Se$_3$ NPs into 10 mM PBS solution (pH 7.0) and data were acquired in the phase analysis light scattering mode at 25 °C. Stability of the Bi$_2$Se$_3$ NPs was also evaluated using light scattering. Bi$_2$Se$_3$ NPs were diluted five times in PBS, and size distribution was measured after 3 month in a 5 mL glass cuvette to check the possible change in size.

Biodistribution: The organs and the solutions from the Bi$_2$Se$_3$ NPs-treated mice were digested by using a microwave system CEM Mars 5 (CEM, Kamp Lintfort, Germany). The Bi and Se content were measured with an ICP-MS, type Agilent 7500 CE (Agilent Technologies, Waldbronn, Germany).

Hematology, Biochemistry, and Pathology: Using a standard saphenous vein blood collection technique, blood was drawn for hematology analysis (potassium EDTA collection tube). The analysis of standard hematological and biochemical examination was carried out. For blood analysis, 1 mL of blood was collected from mice and separated by centrifugation into cellular and plasma fractions. Mice were sacrificed by isoflurane anesthetic and angio catheter exsanguinations, and major organs from those mice were harvested, fixed in 10% neutral buffered formalin, processed routinely into paraffin, stained with H&E and pathology were examined by a digital microscope.

In vitro Cytotoxicity Test: Hela cells were cultured at 37 °C in humidified atmosphere with 5% CO$_2$ and high-glucose Dulbecco's modified Eagle's medium (DMEM) which contained fetal calf serum (10%), L-glutamine (2.9 mg/mL), streptomycin (1 mg/mL), and penicillin (1000 units/mL). The cells (in culture medium) were dispensed in 96-well plates (90 µL containing 6000 cells per well). Different concentrations of the Bi$_2$Se$_3$ NPs (10 µL) were then added to each well. The effect of the concentration of Bi$_2$Se$_3$ NPs was assessed using MTT Cell Proliferation and Cytotoxicity Assay Kit. After 24 or 48 h of treatment, 10 µL of MTT reagent was added and incubate for 4 h, then the medium were replaced with 150 µL DMSO. The optical absorption in 490 nm signal was recorded with a single tube luminometer (TD 20/20, Turner Biosystems Inc., Sunnyvale, CA, USA).

In Vivo Toxicity: 64 male C57 mice at 11 weeks of age were obtained from the Institute of Radiation Medicine (IRM) laboratories and were housed by 2 mice per cage in a 12 h/12 h light/dark cycle, and were provided with food and water ad libitum. Mice were randomly divided into eight groups (eight mice in each group): 1 day control, 1 day treated, 7 days control, 7 days treated, 30 days control, 30 days treated, and 90 days control, 90 days treated mice, respectively. A Bi_2Se_3 NPs solution (200 μL, 2 mg/mL) was used for the animal experiment using intraperitoneal injection. The concentration was 20 mg/kg in each mouse. The animals were weighed and assessed every day to check the behavioral changes. After 1, 7, 30, and 90 days treatment, all mice were sacrificed, and blood and organs were collected for biochemistry and pathological studies. Mice were sacrificed using isoflurane anesthetic and angiocatheter exsanguination with PBS. One mouse from each group was fixed with 10% buffered formalin following phosphate-buffered saline exsanguination. During necropsy, liver, kidneys, spleen, heart, lung, testis, brain, bladder, and thymus were collected and weighed. To explicitly examine the grade of changes caused by malities, spleen and thymus indexes (S_x) were used:

$$S_x = \frac{\text{Weight of experimental organ } (mg)}{\text{Weight of experimental animal } (g)}$$

In vitro DNA Break: A modified version of the alkaline COMET-assay protocol was performed to assay the DNA break. In a typical assay, frosted microscope slides were covered with 200 μL of 0.1% agarose in PBS. After the solidification of agarose, 2×10^5 cells suspended in 10 μL of PBS and 75 μL of 0.5% low-melting-point agarose were added to each slide. After solidification, the slides were placed in cold fresh lyses buffer [2.5 M NaCl, 100 mM disodium ethylenediaminetetraacetate (EDTA), 10 mM Tris-HCl, and 1% Triton X-100] for 1 h and subsequently in a horizontal gel electrophoresis unit (20 × 25 cm) filled with chilled electrophoresis buffer (300 mM NaOH and 1 mM Na_2EDTA) for 30 min. Electrophoresis was then conducted at 14 V for 1 h. The slides were drained, neutralized, and dried with ethanol after the electrophoresis. The comets were stained with ethidium bromide. The DNA damage was analyzed using Comet Assay Software Project (CASP) software that measures the tail moment.

In vitro Radiation Therapy: Hela cells were incubated in 96-well plates (6000 per well) overnight and then exposed to the Bi_2Se_3 NPs (100 μL, 200 μg/mL) for another 24 h. Then, the cells were irradiated under gamma rays from ^{137}Cs (photon energy 662 keV) with an activity of 3600 Ci at the doses of 1, 2, 4, 6, and 8 Gy. After 24 h of irradiation, cells viability was measured by MTT assay.

In vivo Radiation Therapy: All animals were purchased, maintained, and handled using protocols approved by the Institute of Radiation Medicine (IRM) at the Chinese Academy of Medical Sciences (CAMS). The U14 tumor models were generated by subcutaneous injection of 2×10^6 cells in 50 μL PBS into the right shoulder of female BALB/c mice. The mice were treated with the PVP-protected Bi_2Se_3 NPs when the tumor volume reached 100–130 mm^3 (7 days after tumor inoculation). For control, 200 μL saline was injected into mice via intraperitoneal injection. For the treatment, 2 mg/mL of the Bi_2Se_3 NPs was used for the animal experiment, and the concentration was raised up to 20 mg/kg in the mice. Subsequently, the mice were radiated by 5 Gy gamma rays, and ^{137}Cs with activity of 3600 Ci and photon energy of 662 keV were used. 32 mice were assigned to the following groups (eight mice in each group): control, the PVP-protected Bi_2Se_3 NPs, radiation alone, the Bi_2Se_3 NPs plus radiation. The tumor size was measured every two or three days and calculated as: volume = (tumor length) × (tumor width)^2/2.

Statistical Analysis: All data presented in this study are the average ± SD of at least three or more experimental results. The paired Student's t-test was used for the statistical analysis.

Supporting Information

Supporting Information is available from the Wiley Online Library or from the author.

Acknowledgements

[1] H. Zhang, C. X. Liu, X. L. Qi, X. Dai, Z. Fang, S. C. Zhang, *Nat. Phys.* **2009**, *5*, 438.

[2] Y. Xia, D. Qian, D. Hsieh, L. Wray, A. Pal, H. Lin, A. Bansil, D. Grauer, Y. Hor, R. Cava, M. Z. Hasan, *Nat. Phys.* **2009**, *5*, 398.

[3] M. Z. Hasan, C. L. Kane, *Rev. Mod. Phys.* **2010**, *82*, 3045.

[4] Y. Chen, J. Analytis, J.-H. Chu, Z. Liu, S. K. Mo, X. L. Qi, H. Zhang, D. Lu, X. Dai, Z. Fang, S. C. Zhang, I. R. Fisher, Z Hussain, Z. X. Shen, *Science* **2009**, *325*, 178.

[5] D. Hsieh, D. Qian, L. Wray, Y. Xia, Y. S. Hor, R. Cava, M. Z. Hasan, *Nature* **2008**, *452*, 970.

[6] X. L. Qi, S. C. Zhang, *Rev. Mod. Phys.* **2011**, *83*, 1057.

[7] D. Hsieh, Y. Xia, L. Wray, D. Qian, A. Pal, J. Dil, J. Osterwalder, F. Meier, G. Bihlmayer, C. Kane, *Science* **2009**, *323*, 919.

[8] L. Kong, Q. Yuan, H. Zhu, Y. Li, Q. Guo, Q. Wang, X. Bi, X. Gao, *Biomaterials* **2011**, *32*, 6515.

[9] J. F. Hainfeld, D. N. Slatkin, H. M. Smilowitz, *Phys. Med. Biol.* **2004**, *49*, N309.

[10] W. N. Rahman, N. Bishara, T. Ackerly, C. F. He, P. Jackson, C. Wong, R. Davidson, M. Geso, *Nanomed. Nanotechnol.* **2009**, *5*, 136.

[11] D. B. Chithrani, S. Jelveh, F. Jalali, M. van Prooijen, C. Allen, R. G. Bristow, R. P. Hill, D. A. Jaffray, *Radiat. Res.* **2010**, *173*, 719.

[12] Y. J. Li, A. L. Perkins, Y. Su, Y. Ma, L. Colson, D. A. Horne, Y. Chen, *Proc Natl. Acad. Sci. USA* **2012**, *109*, 4092.

[13] X. D. Zhang, D. Wu, X. Shen, J. Chen, Y. M. Sun, P. X. Liu, X. J. Liang, *Biomaterials* **2012**, *33* 6408.

[14] A. E. Nel, L. Mädler, D. Velegol, T. Xia, E. M. Hoek, P. Somasundaran, F. Klaessig, V. Castranova, M. Thompson, *Nat. Mater.* **2009**, *8*, 543.

[15] Y. Zhao, X. Sun, G. Zhang, B. G. Trewyn, I. I. Slowing, V. S. Y. Lin, *ACS Nano* **2011**, *5*, 1366.

[16] A. Albanese, P. S. Tang, W. C. Chan, *Annu. Rev. Biomed. Eng.* **2012**, *14*, 1.

[17] B. Wang, X. He, Z. Zhang, Y. Zhao, W. Feng, *Acc. Chem. Res.* **2013**, *46*, 761.

[18] A. Verma, F. Stellacci, *Small* **2009**, *6*, 12.

[19] C. J. Murphy, A. M. Gole, J. W. Stone, P. N. Sisco, A. M. Alkilany, E. C. Goldsmith, S. C. Baxter, *Acc. Chem. Res.* **2008**, *41*, 1721.

[20] P. Rivera-Gil, D. Jimenez De Aberasturi, V. Wulf, B. Pelaz, P. Del Pino, Y. Zhao, J. M. De La Fuente, I. Ruiz De Larramendi, T. Rojo, X. J. Liang, W. J. Parak, *Acc. Chem. Res.* **2012**, *46*, 743.

[21] A. Nel, T. Xia, L. Mädler, N. Li, *Science* **2006**, *311*, 622.

[22] D. Hühn, K. Kantner, C. Geidel, S. Brandholt, I. De Cock, S. J. Soenen, P. Rivera-Gil, J. M. Montenegro Martos, K. Braeckmans, K. Mullen, G. U. Nienhaus, M. Klapper, W. J. Parak, *ACS Nano* **2013**, *7*, 3253.

[23] E. C. Cho, Q. Zhang, Y. Xia, *Nat. Nano.* **2011**, *6*, 385.

[24] S. H. D. P. Lacerda, J. J. Park, C. Meuse, D. Pristinski, M. L. Becker, A. Karim, J. F. Douglas, *ACS Nano* **2009**, *4*, 365.

[25] W. Jiang, B. Y. Kim, J. T. Rutka, W. C. Chan, *Nat. Nano.* **2008**, *3*, 145.

Materials Views

www.MaterialsViews.com

ADVANCED
FUNCTIONAL
MATERIALS

www.afm-journal.de

FULL PAPER

[26] B. D. Chithrani, A. A. Ghazani, W. C. Chan, *Nano Lett.* **2006**, *6*, 662.

[27] B. D. Chithrani, W. C. Chan, *Nano Lett.* **2007**, *7*, 1542.

[28] Y. Pan, S. Neuss, A. Leifert, M. Fischler, F. Wen, U. Simon, G. Schmid, W. Brandau, W. Jahnen-Dechent, *Small* **2007**, *3*, 1941.

[29] W. H. De Jong, W. I. Hagens, P. Krystek, M. C. Burger, A. J. Sips, R. E. Geertsma, *Biomaterials* **2008**, *29*, 1912.

[30] H. Meng, M. Xue, T. Xia, Z. Ji, D. Y. Tarn, J. I. Zink, A. E. Nel, *ACS nano* **2011**, *5*, 4131.

[31] S. Huo, H. Ma, K. Huang, J. Liu, W. Tui, S. Jin, J. Zhang, S. He, X. J. Liang, *Cancer Res.* **2013**, *73*, 319.

[32] S. D. Perrault, C. Walkey, T. Jennings, H. C. Fischer, W. C. Chan, *Nano Lett.* **2009**, *9*, 1909.

[33] J. Chen, D. Wang, J. Xi, L. Au, A. Siekkinen, A. Warsen, Z. Y. Li, H. Zhang, Y. Xia, X. Li, *Nano Lett.* **2007**, *7*, 1318.

[34] J. Chen, C. Glaus, R. Laforest, Q. Zhang, M. Yang, M. Gidding, M. J. Welch, Y. Xia, *Small* **2010**, *6*, 811.

[35] J. Liu, M. Yu, C. Zhou, S. Yang, X. Ning, J. Zheng, *J. Am. Chem. Soc.* **2013**, *135*, 4978.

[36] O. Rabin, J. M. Perez, J. Grimm, G. Wojtkiewicz, R. Weissleder, *Nat. Mater.* **2006**, *5*, 118.

[37] J. Huang, L. Bu, J. Xie, K. Chen, Z. Cheng, X. Li, X. Chen, *ACS nano* **2010**, *4*, 7151.

[38] Z. M. Markovic, L. M. Harhaji-Trajkovic, B. M. Todorovic-Markovic, D. P. Kepić, K. M. Arsikin, S. P. Jovanović, A. C. Pantovic, M. D. Dramićanin, V. S. Trajkovic, *Biomaterials* **2011**, *32*, 1121.

[39] K. Yang, S. Zhang, G. Zhang, X. Sun, S. T. Lee, Z. Liu, *Nano Lett.* **2010**, *10*, 3318.

[40] J. H. Park, L. Gu, G. von Maltzahn, E. Ruoslahti, S. N. Bhatia, M. J. Sailor, *Nat. Mater.* **2009**, *8*, 331.

[41] M. L. Schipper, N. Nakayama-Ratchford, C. R. Davis, N. W. S. Kam, P. Chu, Z. Liu, X. Sun, H. Dai, S. S. Gambhir, *Nat. Nanotechnol.* **2008**, *3*, 216.

[42] H. S. Choi, W. Liu, P. Misra, E. Tanaka, J. P. Zimmer, B. I. Ipe, M. G. Bawendi, J. V. Frangioni, *Nat. Biotech.* **2007**, *25*, 1165.

[43] W.-S. Cho, M. Cho, J. Jeong, M. Choi, H.-Y. Cho, B. S. Han, S. H. Kim, H. O. Kim, Y. T. Lim, B. H. Chung, J. Jeong, *Toxicol. Appl. Pharm.* **2009**, *236*, 16.

[44] C. H. J. Choi, J. E. Zuckerman, P. Webster, M. E. Davis, *Proc Natl. Acad. Sci. USA* **2011**, *108*, 6656.

[45] W. S. Cho, M. Cho, J. Jeong, M. Choi, B. S. Han, H.-S. Shin, J. Hong, B. H. Chung, J. Jeong, M. H. Cho, *Toxicol. Appl. Pharm.* **2010**, *245*, 116.

[46] C. D. Walkey, J. B. Olsen, H. Guo, A. Emili, W. C. Chan, *J. Am. Chem. Soc.* **2012**, *134*, 2139.

[47] M. C. Mancini, B. A. Kairdolf, A. M. Smith, S. Nie, *J. Am. Chem. Soc.* **2008**, *130*, 10836.

[48] Y R. S. Yang, L. W. Chang, J. P. Wu, M.-H. Tsai, H.-J. Wang, Y. C. Kuo, T.-K. Yeh, C. S. Yang, P. Lin, *Environ. Health Persp.* **2007**, *115*, 1339.

[49] L. Ye, K.-T. Yong, L. Liu, I. Roy, R. Hu, J. Zhu, H. Cai, W. C. Law, J. Liu, K. Wang, *Nat. Nanotechnol.* **2012**, *7*, 453.

[50] Y. Min, G. D. Moon, B. S. Kim, B. Lim, U. Jeong, *J. Am. Chem. Soc.* **2012**, *134*, 2872.

[51] Y. Min, J. W. Roh, H. Yang, M. Park, S. I. Kim, S. Hwang, S. M. Lee, K. H. Lee, U. Jeong, *Adv. Mater.* **2013**, *25*, 1425.

[52] K. J. Koski, J. J. Cha, B. W. Reed, C. D. Wessells, D. Kong, Y. Cui, *J. Am. Chem. Soc.* **2012**, *134*, 7584.

[53] A. Guerrero-Martínez, J. Pérez-Juste, L. M. Liz-Marzán, *Adv. Mater.* **2010**, *22*, 1182.

[54] J. Huang, L. Bu, J. Xie, K. Chen, Z. Cheng, X. Li, X. Chen, *ACS Nano* **2010**, *4*, 7151.

[55] E. Sadauskas, H. Wallin, M. Stoltenberg, U. Vogel, P. Doering, A. Larsen, G. Dansche, *Part. Fibre. Toxicol.* **2007**, *4*, 10.

[56] K. Yang, H. Gong, X. Shi, J. Wan, Y. Zhang, Z. Liu, *Biomaterials* **2013**, *34*, 2787.

[57] K. Yang, J. Wan, S. Zhang, Y. Zhang, S. T. Lee, Z. Liu, *ACS Nano* **2011**, *5*, 516.

[58] C. Zhou, M. Long, Y. Qin, X. Sun, J. Zheng, *Angew. Chem.Int. Et.* **2011**, *123*, 3226.

[59] X. D. Zhang, D. Wu, X. Shen, P. X. Liu, F. Y. Fan, S. J. Fan, *Biomaterials* **2012**, *33*, 4628.

[60] H. L. Liu, S. P. Ko, J. H. Wu, M. H. Jung, J. H. Min, J. H. Lee, B. H. An, Y. K. Kim, *J. Magn. Magn. Mater.* **2007**, *310*, 815.

[61] X. D. Zhang, D. Wu, X. Shen, P. X. Liu, N. Yang, B. Zhao, H. Zhang, Y. M. Sun, L. A. Zhang, F. Y. Fan, *Int. J. Nanomed.* **2011**, *6*, 2071.

[62] J. Lipka, M. Semmler-Behnke, R. A. Sperling, A. Wenk, S. Takenaka, C. Schleh, T. Kissel, W. J. Parak, W. G. Kreyling, *Biomaterials* **2010**, *31*, 6574.

[63] S. K. Balasubramanian, J. Jittiwat, J. Manikandan, C. N. Ong, L. E. Yu, W. Y. Ong, *Biomaterials* **2010**, *31*, 2034.

[64] L. Gu, R. H. Fang, M. J. Sailor, J. H. Park, *ACS Nano* **2012**, *6*, 4947.

[65] C. Zhou, G. Hao, P. Thomas, J. Liu, M. Yu, S. Sun, O. K. Öz, X. Sun, J. Zheng, *Angew. Chem. Int. Ed.* **2012**, *124*, 10265.

[66] J. Kaewkhao, P. Limsuwan, *Nucl. Instr. Meth. A* **2010**, *619*, 295.

[67] W. J. Veigele, *Atom. Data. Nucl. Data* **1973**, *5*, 51.

[68] G. Zhang, Z. Yang, W. Lu, R. Zhang, Q. Huang, M. Tian, L. Li, D. Liang, C. Li, *Biomaterials* **2009**, *30*, 1928.

[69] X. Huang, X. Peng, Y. Wang, Y. Wang, D. M. Shin, M.A. El-Sayed, S. Nie, *ACS Nano* **2010**, *4*, 5887.

[70] H. C. Fischer, L. Liu, K. S. Pang, W. C. Chan, *Adv. Funct. Mater.* **2006**, *16*, 1299.

[71] G. von Maltzahn, J. H. Park, A. Agrawal, N. K. Bandaru, S. K. Das, M. J. Sailor, S. N. Bhatia, *Cancer Res.* **2009**, *69*, 3892.

[72] J. T. Robinson, S. M. Tabakman, Y. Liang, H. Wang, H. Sanchez Casalongue, D. Vinh, H. Dai, *J. Am. Chem. Soc.* **2011**, *133*, 6825.

[73] J. T. Robinson, S. M. Tabakman, Y. Liang, H. Wang, H. Sanchez Casalongue, D. Vinh, H. Dai, *J. Am. Chem. Soc.* **2012**, *134*, 10664.

[74] C. Chantler, *J. Phys. Chem. Refer. Data* **2000**, *29*, 597.

[75] C. Alric, J. Taleb, G. L. Duc, C. Mandon, C. Billotey, A. L. Meur-Herland, T. Brochard, F. Vocanson, M. Janier, P. Perriat, *J. Am. Chem. Soc.* **2008**, *130*, 5908.

[76] D. Kim, S. Park, J. H. Lee, Y. Y. Jeong, S. Jon, *J. Am. Chem. Soc.* **2007**, *129*, 7661.